Ion-energy effects in silicon ion-beam epitaxy

J. W. Rabalais,* A. H. Al-Bayati, K. J. Boyd, and D. Marton
Department of Chemistry, University of Houston, Houston, Texas 77204-5641

J. Kulik, Z. Zhang, and W. K. Chu
Department of Physics and Texas Center for Superconductivity, University of Houston, Houston, Texas 77204
(Received 7 December 1995)

Direct ion-beam deposition of $^{28}Si^+$ ions for homoepitaxial film growth on Si{100} has been studied over the ion-energy range of 8–80 eV in the low-temperature range of 40–500 °C. Deposition was performed by means of a mass-selected, low-energy, ultrahigh-vacuum ion-beam system with a well-defined ion energy (E) for which the energy spread is $\Delta E = \pm 3$ eV. The films were analyzed *in situ* at growth intervals by reflection high-energy electron diffraction and Auger-electron spectroscopy, and *ex situ* by cross-section high-resolution transmission electron microscopy, Rutherford backscattering spectrometry, and secondary-ion-mass spectrometry (SIMS) depth profiling. The growth mode, crystalline quality, and number of defects in the films are found to be extremely sensitive to both substrate temperature (at low temperature) and ion energy (at low energy). Layer-by-layer epitaxial growth is observed down to ~160 °C with appropriate ion energies; below this temperature, island growth with a transition to an amorphous phase occurs. An optimum ion-energy window for achieving layer-by-layer epitaxial growth and high crystalline quality films which are relatively defect free is observed. This energy window, which illustrates ion beam enhanced epitaxy, is extremely narrow at low temperature, i.e., ~20±10 eV at 160 °C, and broadens out on the low-energy side at higher temperatures, e.g., at 290 °C. Within this energy window, the films have the same level of crystallinity as the single-crystal silicon substrate. This behavior is discussed in terms of the changes in the phenomena which dominate the growth process as a function of ion energy and temperature. For the conditions 290 °C and 20 eV, epitaxial high crystalline quality films up to 352 nm thick have been grown, and there is no indication of a limiting epitaxial layer thickness. SIMS analysis shows that the isotropic enhancement ratio is $^{28}Si/(^{29}Si + ^{30}Si) > 10^4$.[S0163-1829(96)05316-7]

I. INTRODUCTION

The incessant decrease in silicon device dimensions places great demands on the control of interface widths and doping profiles. It is essential to lower processing temperatures in order to meet these increasingly stringent requirements. The use of hyperthermal particles, either Si^+ ions[1–9] or rare-gas ions,[10–13] in promoting low-temperature silicon homoepitaxy has been demonstrated by several research groups. The kinetic energy of these ions is coupled directly to the growth surface, facilitating local atomic rearrangement and allowing atoms to relax into lower-energy sites. Details of the mechanism of energetic particle enhancement for low substrate temperature epitaxy are not completely understood. It is believed that the optimum low-temperature epitaxial conditions are determined by a delicate balance between the beneficial effects of ion irradiation, such as local relaxation, creation of mobile vacancy/interstitial pairs, and enhanced diffusion, and the undesirable effects, such as permanent defect formation, lattice damage, sputtering, atomic mixing, etc. This balance of the beneficial and undesirable effects can be shifted through control of the ion energy, suggesting that there should be an optimum ion energy for low-temperature epitaxial growth of relatively defect-free films. The purpose of this paper is to present data which reveal that there is such an optimum ion energy for low-temperature silicon homoepitaxy, and that its value is related to the interplay between local atomic rearrangements, surface diffusion, and lattice displacement energy. A sharp minimum in the defect density of silicon films as a function of Si^+ ion deposition energy is observed. We demonstrate that high crystalline quality, isotopically pure, epitaxial silicon films with sharp film-substrate interfaces can be grown at low temperature through careful control of the Si^+ ion energy.

Direct ion-beam deposition of thin films, i.e., self-ion deposition, was demonstrated some 25 years ago.[14,15] Since that time, research groups[1–24] throughout the world have shown that the use of such hyperthermal or energetic particles for film deposition has a strong influence on the film growth kinetics and the resulting physical properties of metal, semiconductor, and compound films. Some of the beneficial effects observed include film densification, low-temperature epitaxial growth, enhanced film-substrate adhesion, growth of metastable phases, stimulation of chemical reactions, control of film stoichiometry for compound films, and increased dopant incorporation. However, these desirable results are often overshadowed by the deleterious effects introduced by the energetic particles themselves. The understanding of these complex processes which occur during hyperthermal or energetic ion deposition of films has improved in recent years due to carefully controlled experiments and the use of ion trajectory simulations[25,26] and molecular-dynamics calculations.[27–34]

Previous studies of direct low-temperature Si^+ ion-beam epitaxy (IBE) have generated optimism about the possibility of film growth under conditions where intermixing and dop-

ant migration are negligible. For example, the Oak Ridge group[2–4] has used IBE to demonstrate silicon homoepitaxy down to 375 °C with 30-eV Si^+, amorphous Si and Ge heterostructures, self-ion sputter cleaning, and reactive ion cleaning. The Salford group[5] has shown that the crystalline quality of silicon films improves monotonically as ion energy is decreased from 100 to 10 eV for substrate temperatures $\geq$350 °C. Matsuoka and Tohno[9] have shown that films with the same level of crystallinity as bulk single-crystal silicon can be grown at 320°C for Si^+ ion energies less than 25 eV; the defect density increased drastically for energies above 50 eV. The results from all three of these groups have provided insight into near-surface radiation damage effects caused by low-energy ions in silicon homoepitaxy, and consistently show that the epitaxial quality of the films decreases rapidly as primary energies increase above the atomic displacement threshold. Our research group[6,7] has demonstrated layer-by-layer epitaxial growth at 290 °C using 15-eV Si^+, the deleterious effects of contamination on epitaxial growth, and the strong energy and temperature dependence of the crystal quality of the films.

Other techniques have been used in studying Si epitaxy at low temperature; we will only discuss those that are closely related to this study. Molecular-beam epitaxy (MBE) studies[35–37] of Si film growth at low temperature have shown that the films become amorphous after a certain epitaxial layer thickness (h_{epi}); h_{epi} decreases with decreasing temperature. The failure of the epitaxy is not well understood; however, it has been suggested[36–38] that it may be due to increased roughening during epitaxy and/or hydrogen stabilization of defects during growth. Murty *et al.*,[10] have shown that concurrent Ar^+ ion irradiation during silicon MBE increases h_{epi} at temperatures $>$300 °C relative to conventional MBE. The crystalline quality of Si films deposited from a plasma-sputtering system at 300 °C was found[9–11] to be dependent on the energy of the Ar^+ ions; device quality films can be obtained at the optimum conditions.

The studies cited above lead to the following questions. Can the ion energy in direct ion-beam epitaxy (IBE) be used to enhance the local relaxation of adatoms and desorption of impurities, both of which are reduced at low temperature, in order to maintain and improve epitaxial growth at low temperature? Is there an optimum ion energy for low-temperature Si^+ IBE of high crystalline quality films? The data that we present herein provide answers to these questions. These data consist of the variation in crystalline quality of silicon homoepitaxial films grown by direct $^{28}Si^+$ IBE in the temperature range of 40–500 °C and the ion-energy range of 8–80 eV. The sharp ion-energy distribution of the beam allows the investigation of detailed changes as a function of ion energy. The crystalline structure of the films was analyzed by *in situ* reflection high-energy electron diffraction (RHEED), and *ex situ* Rutherford backscattering spectrometry (RBS) and cross-section high-resolution transmission electron microscopy (TEM). Impurities in the films were monitored by *in situ* Auger-electron spectroscopy (AES). The isotropic purity of the films was determined by secondary-ion-mass spectrometry (SIMS) depth profiling.

II. EXPERIMENTAL PROCEDURES

A. Ion-beam deposition of silicon

Silicon films were grown by direct $^{28}Si^+$ deposition on Si{100} surfaces by means of a dual-source, mass-selected, low-energy ion-beam instrument which has been described elsewhwere.[39] Briefly, the system consists of two Freeman ion sources, two laminated magnets, and a retarding lens. The first magnet with dual sectors is for isotope separation, while the second one is for elimination of high-energy neutrals and for focusing the beam on target. Only one ion source is used for this particular study. The ions are accelerated to 10 keV, transported at this energy through the beam line, and retarded to the specific ion energy on a grounded target. The energy profile of the beam has a Gaussian shape with a full width at half maximum (FWHM) of ± 3 eV.[39] The unscanned beam has a ribbonlike shape, flat over 10–15 mm along the vertical axis with a Gaussian-like shape where the FWHM equals 3–5 mm along the horizontal axis. This FWHM is increased to 8–10 mm, and uniformity is improved by scanning the beam horizontally. The current density of the scanned 15-eV $^{28}Si^+$ beam was 1–2 μA cm^{-2}, corresponding to a deposition rate of 0.7–1.4 Å min^{-1}. The current density at the center (maximum current) was used for dose calculations. The base and beam-on-target pressures of the ultrahigh-vacuum (UHV) deposition chamber, pumped by means of two turbomolecular pumps, an ion pump, and a titanium sublimation pump, were 1×10^{-9} and 5×10^{-9} mbar, respectively. Sample temperatures were measured by means of a pyrometer and a thermocouple which was attached to the sample; the pyrometer readings were calibrated by the thermocouple. The absolute temperature measurements for the range studied, i.e., 40–500 °C, have a maximum error of $\pm$20 °C.

B. Preparation of silicon substrate surface

The silicon substrates were Si(100) wafers (CZ, *p*-type, B-doped, 10–20 Ω cm) which were cleaved to $\sim 1\times 1$-cm^2 samples. For the SIMS measurements, undoped wafers of resistivity 10 kΩ cm were used. Since the purpose of this work is to study the effects of ion energy on film growth, we used a silicon substrate surface that was atomically clean and well ordered. Such silicon surfaces were prepared using the well-known high-temperature (1200 °C) annealing method.[40] Sample heating up to 1200 °C was achieved by radiative heating and electron bombardment from a tungsten filament mounted behind the substrate. The cleaning procedure used was as follows: The substrates were cleaned ultrasonically with acetone twice. After transferring the sample from the load lock chamber into the deposition chamber, the temperature was increased slowly to ~300 °C, to 600 °C, and then to 900 °C, and maintained at each of these temperatures for a few hours to allow sufficient time for outgassing. Finally the temperature was increased to 1200 °C in a few minutes, maintained at 1200 °C for 30 s, and then decreased to the deposition temperature at a rate of ~2 °C/s. Auger-electron spectra of such surfaces exhibited no detectable impurities. Clear, spotty (2×1) RHEED patterns, indicative of (2×1) reconstruction,[41] were observed from these clean surfaces. It should be mentioned that films deposited on surfaces cleaned by HF etching followed by annealing to 450 °C in vacuum were highly defective, consistent with previous results;[5] these results are not discussed further in this paper.

C. Film characterization

The initial silicon substrate surface and deposited films were characterized *in situ* by static RHEED and AES, and *ex situ* by RBS, cross-section high-resolution TEM, and SIMS depth profiling. The RHEED patterns were measured immediately after each incremental dose was applied, with the sample at the deposition temperature, using a 30-keV electron beam incident along the $\langle 110 \rangle$ direction and a grazing incidence angle of $\sim 0.8°$. For this angle, the beam diameter of 100 μm measured at normal incidence is expected to spread over 7 mm along the beam axis. The AES analyses were obtained with a 3-keV electron beam and a cylindrical mirror electron analyzer. RBS and channeling analyses were carried out with a 1.6-MeV He^+ beam, normal angle of incidence ($\langle 100 \rangle$ direction), and a grazing scattering angle of 95°. Since a true random level is difficult to obtain at grazing scattering angles from a virgin sample, RBS data from an amorphous layer were used as a reference for the random level. This amorphous layer was prepared by bombarding a silicon substrate with 9-keV Si^+ to a dose of 4×10^{16} ion cm^{-2} at room temperature. The TEM micrographs were obtained with a 200-keV electron beam. Samples for cross-section TEM analysis were prepared by mechanical thinning to 30 μm followed by 5-keV Ar^+ milling at 12° with respect to the specimen surface. The specimen was cooled with liquid N_2 during this procedure in order to prevent solid phase epitaxial regrowth. The SIMS depth profiles were obtained by sputtering with a 10-keV Cs^+ ion beam.

III. RESULTS

A. RHEED results

RHEED patterns were recorded as a function of Si^+ ion dose at several different temperatures and ion energies. These RHEED patterns were used to obtain a qualitative analysis of the type of film growth and the crystallinity of the deposited film. The coverages in monolayers (1 ML $\sim 6.8\times10^{14}$ atoms cm^{-2}) were calculated from the ion dose, assuming no sputtering and a unity sticking coefficient. These coverages were also calibrated from the SIMS depth profiles. A typical RHEED pattern and AES spectrum for a Si(100) substrate after cleaning at 1200 °C are shown in Fig. 1. The RHEED data show clear spots with a half-order reflection pattern, indicating that the surface is atomically well ordered with 2×1 reconstruction. The observation of spots rather than streaks implies that the surface is smooth and relatively free of protrusions, kinks, etc. From the AES spectrum it can be seen that the C and O signals are below the detection limit.

1. RHEED patterns as a function of temperature

Examples of RHEED patterns observed for deposition with $E=15$ and 20 eV at different temperatures are shown in Figs. 2 and 3, respectively, for selected Si^+ ion doses. After a dose of about 1 ML, the half-order spots of the clean Si (2×1) surface (Fig. 1) disappeared, and streaky (2×1) patterns with surface spots at the ends of the first-order streaks [or three-dimensional (3D) spots] were observed. For $T=40$ and 80 °C, 3D elongated spots with hollow specular reflection were observed at low dose, along with a diffuse

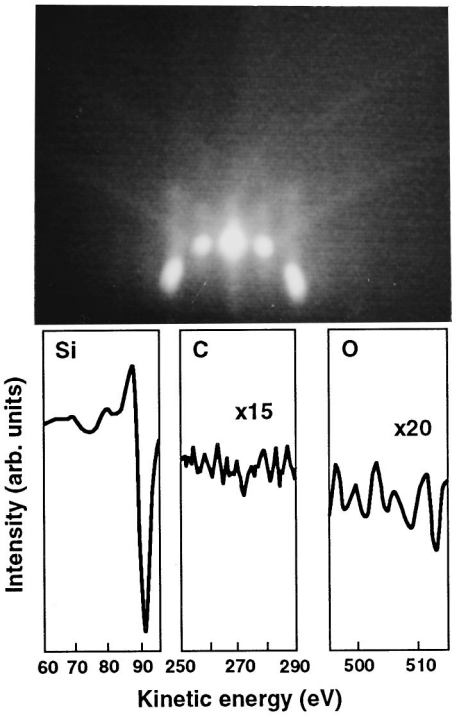

FIG. 1. (Upper figure) Spotty 2×1 RHEED pattern for a Si(100) surface after annealing at 1200 °C. (Lower figure) AES spectrum for this same surface. Note that the C and O signals are within the noise level.

background which increases as a function of dose; this background dominates and produces completely diffuse images at higher doses. This indicates that three-dimensional islands were formed initially, followed by transition to an amorphous phase at higher doses. For $T=120$ and 160 °C, the streaky first-order patterns (half-order streaks were not observed) with 3D spots are persistent at higher doses, although the diffuse background is noticeable. This background does not dominate, as it does at the lower temperatures. At $T=290$ °C, clear, streaky (1×2) patterns are observed up to the highest doses used, which was about 325 nm for some of the thickest films. The observation of streaks indicates that the films grow epitaxially, layer by layer, with the evolving surface containing steps and defects.

2. RHEED patterns as a function of ion energy

Examples of RHEED patterns observed for deposition at 160 °C at different ion energies are shown in Fig. 4 for selected Si^+ doses. At 20 eV, a clear, streaky (2×1) pattern is produced at all doses. For energies less than or greater than 20 eV, streaky patterns with spots are observed initially and the diffuse background increases with dose; these images become completely diffuse when the films are only 60–90 ML thick. These results indicate that at 160 °C there is an optimum ion-energy window for achieving layer-by-layer epitaxial growth, and that this window is in the range of 10–40 eV.

B. High-resolution transmission electron microscopy (TEM) results

Examples of high resolution TEM micrographs of four $\sim$20-nm-thick silicon films deposited under the T/E condi-

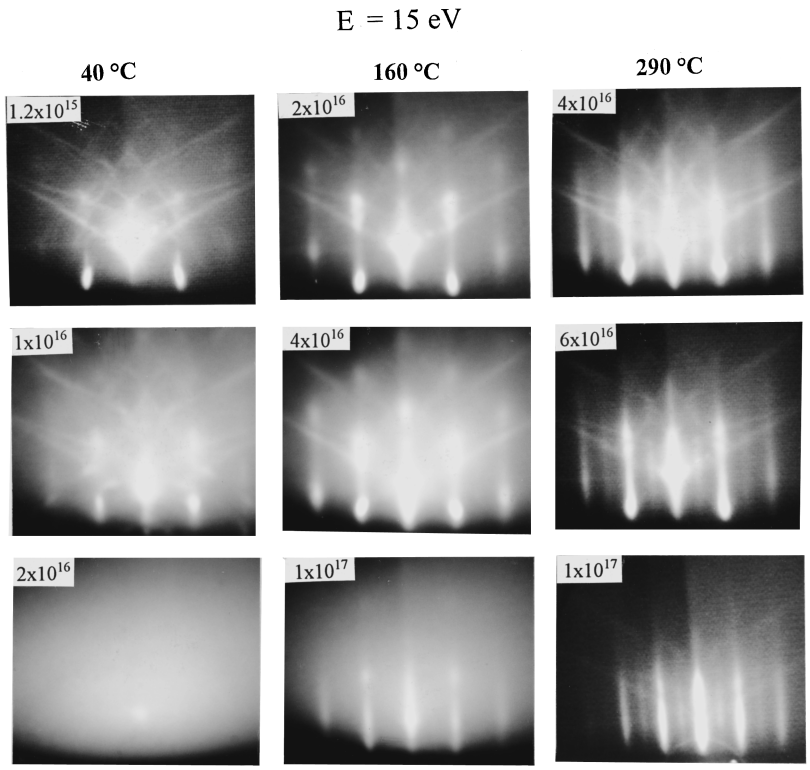

FIG. 2. RHEED patterns for silicon films deposited with a $^{28}Si^{+}$ ion energy of 15 eV at three different substrate temperatures and different ion doses (ions cm^{-2}). Note that at 50 °C the film becomes amorphous at low dose, while at 160 and 290 °C it remains crystalline at the highest doses used. The 290 °C film exhibits the lowest background and clearest pattern.

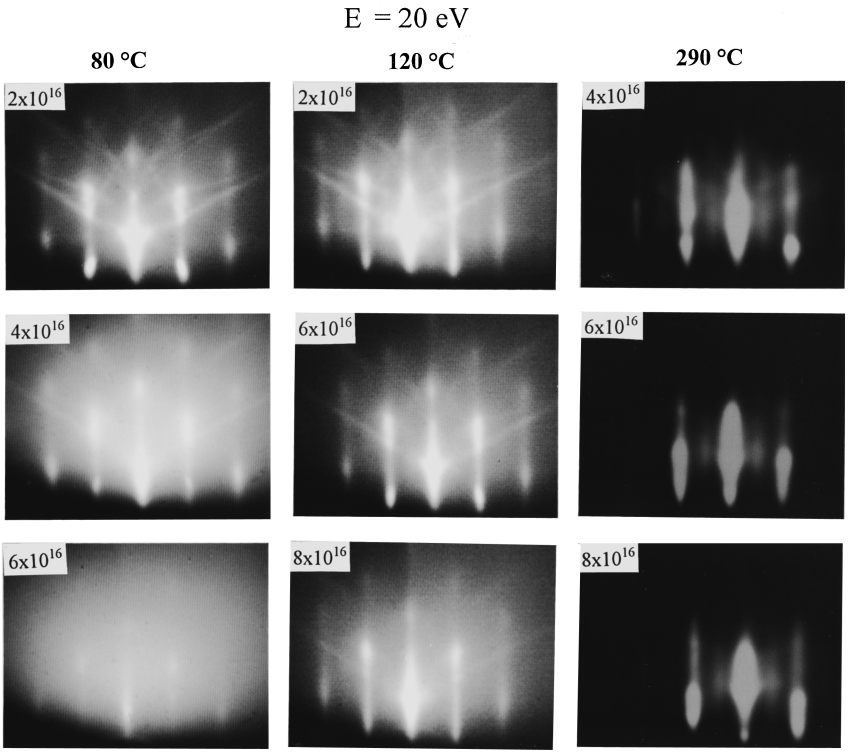

FIG. 3. RHEED patterns for silicon films deposited with a $^{28}Si^{+}$ ion energy of 20 eV at three different substrate temperatures and different ion doses (ions cm^{-2}). Note that at 80 °C the film becomes amorphous at low dose, while at 200 and 290 °C it remains crystalline at the highest doses used. The 290 °C film exhibits the lowest background and clearest pattern.

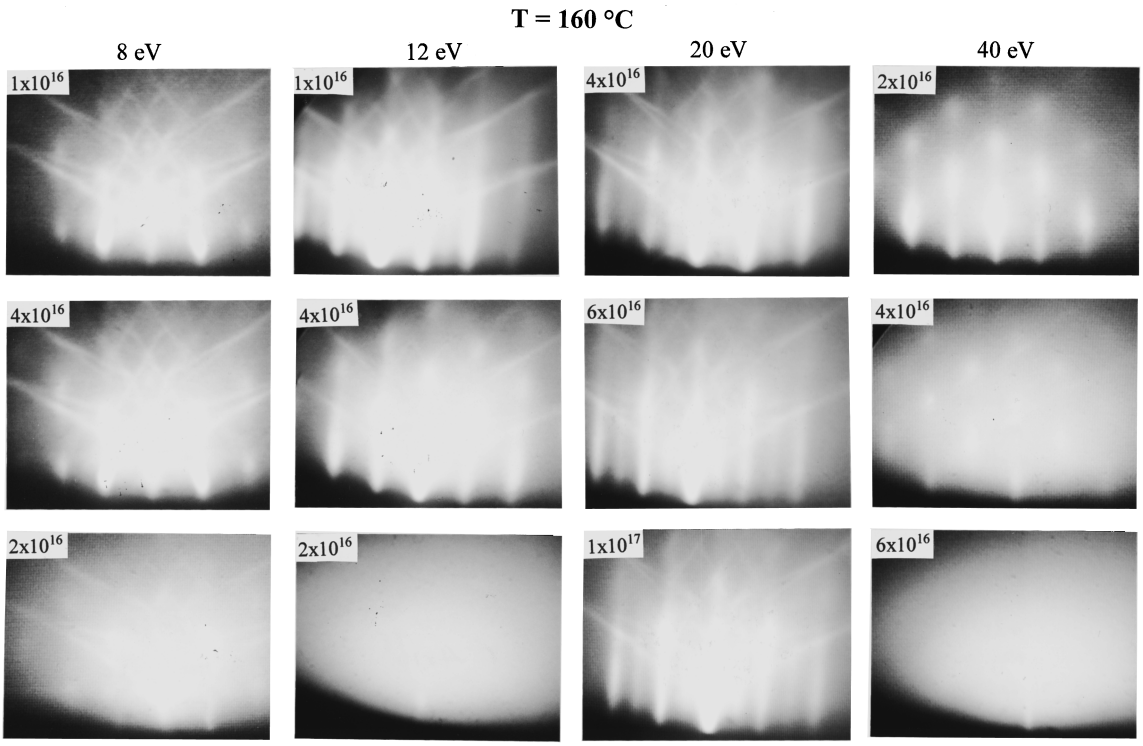

FIG. 4. RHEED patterns for silicon films deposited with a substrate temperature of 160 °C at four different $^{28}Si^{+}$ ion energies and different ion doses (ions cm^{-2}). Note that the 20-eV film remains crystalline at the highest doses used, while the other films become amorphous at lower doses.

tions of 160 °C/15 eV, 160 °C/20 eV, 160 °C/25 eV, and 290 °C/15 eV are shown in Figs. 5–8, respectively.

1. TEM of highly defective films

Consider the 160 °C/15-eV film of Fig. 5. This micrograph shows that the ~16-nm-thick film initially grows epitaxially but eventually becomes noncrystalline at thicknesses greater than ~12 nm. The crossover region is visible as a dark band of zigzag shape in the figure. Lattice fringes are still visible in this region and up to the film surface, indicating that there is still a significant degree of crystallinity. The dark contrast is likely due to a high concentration of point defects or clusters which introduce strain and consequent incoherent scattering of the electron beam to higher angles, and some loss of the lattice fringe signal. There is good agreement with RHEED observations, which showed streaky patterns with 3D spots at lower doses, and images dominated by diffuse background at higher doses. These results indicate that the initial growth is characterized by formation of 3D islands. The stress built up in the film during this phase, as a result of accumulation of defects, is related by a transition to the amorphous phase at higher thickness. The roughness of this strained layer is also visible on the 50-nm scale inset.

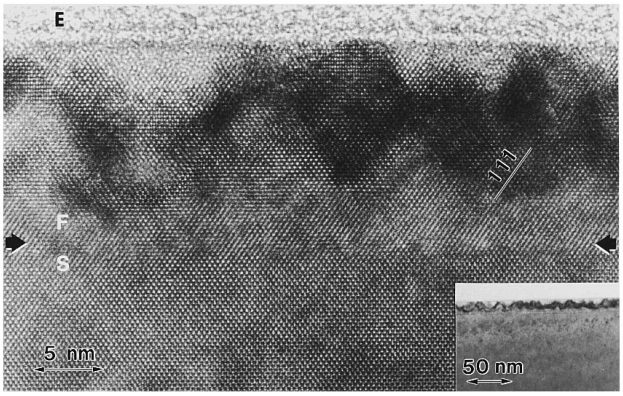

FIG. 5. High-resolution cross-section TEM micrograph for the film deposited at 160 °C using 15-eV $^{28}Si^{+}$ ions. All TEM analyses were performed with the electron beam perpendicular to the (110) plane. Note the formation of a heavily strained layer after a certain epitaxial thickness, beyond which amorphous zones are formed. *F*, film; *S*, substrate; and *E*, epoxy.

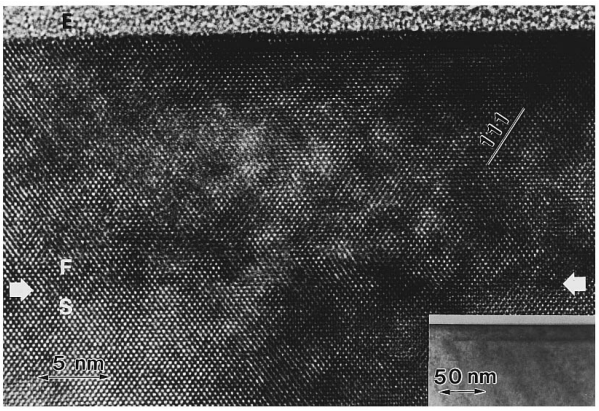

FIG. 6. High-resolution cross-section TEM micrograph for the film deposited at 160 °C using 20-eV $^{28}Si^{+}$ ions. Note the high crystalline quality, lack of observable defects, and continuity of the (111) planes through the interface. *F*, film; *S*, substrate; and *E*, epoxy.

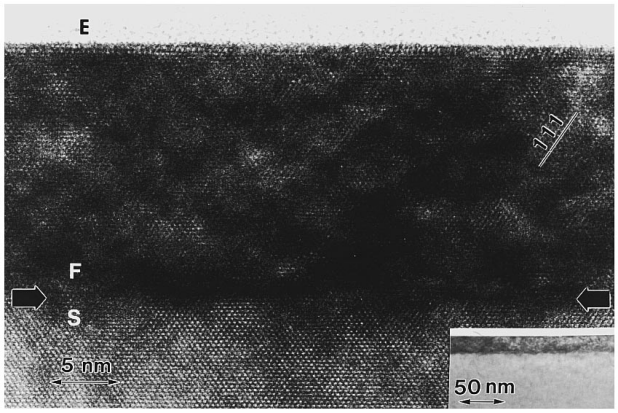

FIG. 7. High-resolution cross-section TEM micrograph for the film deposited at 160 °C using 25-eV $^{28}Si^{+}$ ions. Note the formation of a heavily strained layer after a certain epitaxial thickness, beyond which amorphous zones are formed. *F*, film; *S*, substrate; and *E*, epoxy.

For films grown with the conditions 40 °C/15 eV, the TEM result showed that the transition to the amorphous phase occurs at a much lower thickness (<1 nm), in agreement with the RHEED results. The 160 °C/20-eV film of Fig. 6 exhibits similar characteristics to the 160 °C/15-eV film of Fig. 5; i.e., it is highly strained and has both crystalline and amorphous regions.

2. TEM of high crystalline quality films

Consider the 160 °C/25-eV and 290 °C/15-eV films of Figs. 7 and 8, respectively. Both images exhibit good continuity to the substrate, i.e., there is no observable bending of the (111) planes throughout the substrate and film. In addition, sharp interfaces, no discernible defects in the films, and smooth surfaces are observed. The interface can be seen by the difference in contrast of the film and substrate. This difference in contrast may be attributed to the strain induced by the defects in the film. The RHEED patterns of these films exhibit the streaky (2×1) characteristics of layer-by-layer growth. The surfaces and interfaces are also smooth in the 50-nm scale insets. There is no evidence of damage to the underlying silicon substrate in these insets. Indeed, we carried out systematic TEM observations of the substrates using conventional two-beam imaging conditions, and found no evidence of damage. These results illustrate that silicon films of high crystalline quality can be obtained at low substrate temperatures using IBE.

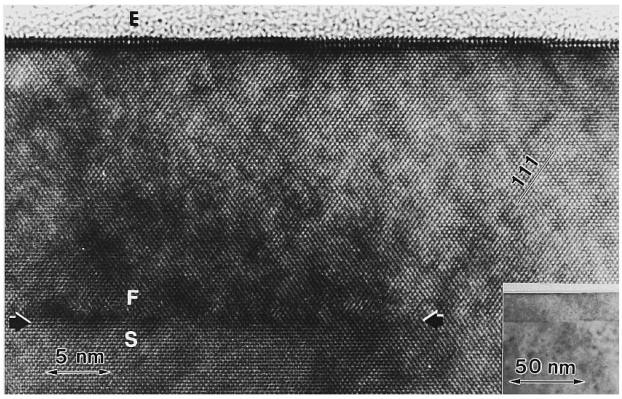

FIG. 8. High-resolution cross-section TEM micrograph for the film deposited at 290 °C using 15-eV $^{28}Si^{+}$ ions. Note the high crystalline quality, lack of observable defects, and continuity of the (111) planes through the interface. *F*, films; *S*, substrate; and *E* epoxy.

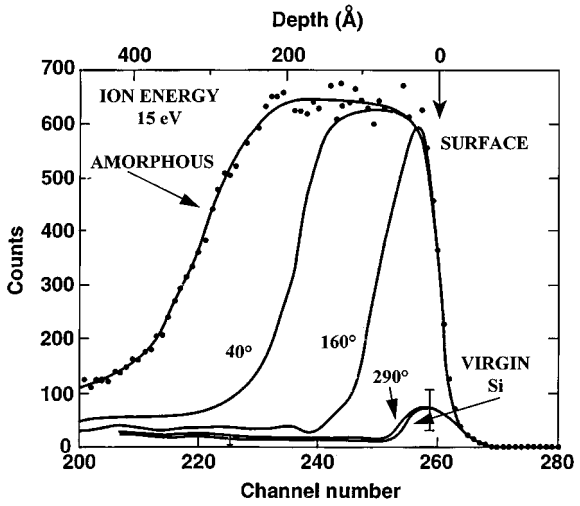

FIG. 9. RBS and channeling spectra for films deposited using 15-eV $^{28}Si^{+}$ ions at substrate temperatures of 40, 160, and 290 °C. The spectra for the virgin silicon substrate and an amorphous silicon sample are plotted for comparison. Experimental points are included only for the amorphized sample in order to avoid confusion; for the other spectra, the best-fit lines are drawn through the data points. The size of the error bars is indicated on the figure.

C. RBS results

Examples of RBS spectra of films deposited at 15 eV as a function of substrate temperature are shown in Fig. 9, and spectra of films deposited at 160 °C as a function of ion energy are shown in Fig. 10. Ion doses of 1×10^{17} ions cm^{-2} were used for all of these depositions, resulting in film thicknesses of ~20 nm. The surface peak for virgin silicon represents the scattering level from the surface atoms of the silicon wafer. Although the wafer was cleaned according to the procedure described in Sec. II B, it was exposed to air prior to the RBS measurement (as were all of the samples) and therefore contains surface oxide. The sizes of the surface peaks for virgin silicon are different in the two figures because of different alignments and normalizations for the two sets of measurements. These alignments and normalizations are consistent within each figure. The height and width (FWHM) of the spectrum of the amorphous surface represent the random level of backscattering and the thickness of the amorphous layer, respectively. The peak width of this spectrum, corresponding to a thickness of 340 Å, was used to convert the energy scale to a depth scale using energy-loss data of 1.6-MeV He^{+} in silicon for the conversion. A quantitative measure of the number of defects (N_d) in the film relative to the virgin substrate was obtained from the number of atoms detected in the RBS Si surface peak. The N_d was defined as $N_d=(N_f-N_s)$, where N_f and N_s refer to the number of atoms in the surface peak of the deposited film and the virgin substrate, respectively.

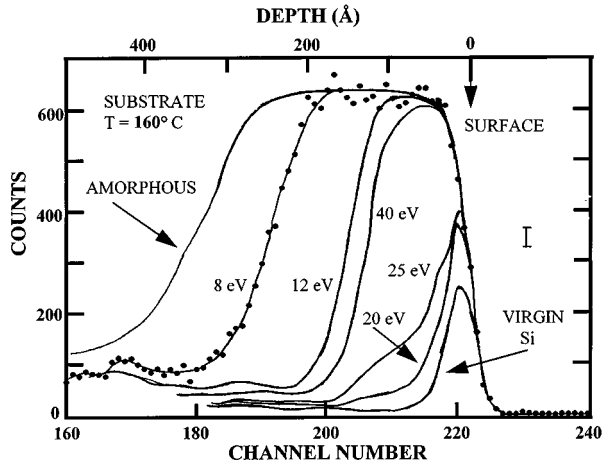

FIG. 10. RBS and channeling spectra for films deposited with a substrate temperature of 160 °C using $^{28}Si^{+}$ ion energies of $E=8$, 12, 20, 25, and 40 eV. The spectra for the virgin silicon substrate and an amorphous silicon sample are plotted for comparison. Experimental points are included only for the 8-eV sample in order to avoid confusion; for the other spectra, the best-fit lines are drawn through the data points. The size of the error bars is indicated on the figure.

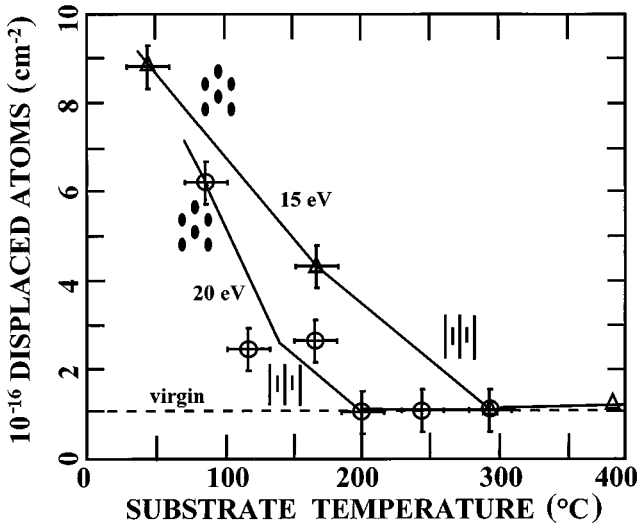

FIG. 11. Plot of the number of displaced atoms (N_d) in the silicon films vs substrate temperature for films deposited with $^{28}Si^{+}$ ion energies of 15 and 20 eV. Qualitative sketches of RHEED patterns observed durig growth are also shown. The number of displaced atoms observed in the virgin spectrum is 1×10^{16} cm^{-2}.

1. RBS as a function of temperature

From Fig. 9 we observe that the number of defects in the films deposited with a constant ion energy of 15 eV is a strong function of substrate temperature. The spectrum for the film deposited at 290 °C is very similar to that for the virgin sample; the surface peak and the dechanneling level for the film are only slightly higher than that of the virgin sample. The extra area under the peak corresponds to $1/6\times10^{15}$ atoms cm^{-2}, indicating that ~1.6% of the atoms deposited did not register epitaxally. The spectra of the films deposited at 160 and 40 °C reach the random level. This indicates that highly defective films with amorphous regions were formed at these temperatures. The surface peak for 40 °C is wider than that for 160 °C, signifying that a thicker amorphous layer is formed at the lower temperature. Since the films and the substrate have the same mass, it is difficult to identify the film-substrate interface from the RBS spectra. However, since the film deposited at 40 °C became amorphous at a dose of less than 2×10^{16} ions/cm^{-2}, the trailing edge of the surface peak can be used to estimate the position of the interface for all of the films. Assuming that 8×10^{16} atoms cm^{-2} of the film is amorphous, this gives an amorphous layer thickness of 160 Å, in good agreement with that obtained from the FWHM of the spectrum, i.e., 188 Å. These results are consistent with the more qualitative results from the RHEED measurements, which suggest 3D island formation at low temperature, and from the TEM measurements, which show that these films are initially highly strained and epitaxial before becoming amorphous. The RBS scattering yield from epitaxial 3D islands will be reduced due to the channeling effect. Since the thickness of the 3D epitaxial layer of the film grown at 160 °C is larger than that of the film grown at 40 °C, the scattering yield for the 160 °C film will be lower than that for the 40 °C film.

In order to probe the effect of temperature on the quality of the IBE films, the number of defects N_d in the films was determined by RBS for ~20-nm-thick films deposited at 15 and 20 eV over the range 40–290 °C. The results are plotted in Fig. 11. Sketches of the corresponding RHEED images observed during growth are also indicated in the figure. These sketches serve only as a qualitative guide to the RHEED observations; the 3D spots are actually elongated along the vertical direction. N_d decreases as a function of temperature until it reaches the level of the virgin substrate at ~200 and ~290 °C for 20 and 15 eV, respectively. The N_d for 15 eV remains higher than that for 20 eV until it reaches the level of the substrate at higher temperature. The 3D spots observed at low temperature become streaky patterns at higher temperatures, where N_d approaches the substrate level.

2. RBS as a function of ion energy

Figure 10 shows that the number of defects in the deposited films is highly sensitive to the ion energy used for deposition at a substrate temperature of 160 °C. The 20-eV sample has the smallest surface peak, corresponding to the minimum misalignment of deposited atoms. The area of this peak shows that ~8% of the deposited atoms relative to the virgin surface peak are not registered epitaxially. The intensities and widths of the surface peaks increase as ion energy either decreases below or increases above 20 eV. The peak height of the random level is attained for both the 12- and 40-eV films. The energy dependence is remarkably sharp, particularly on the low-energy side of 20 eV. The width of the 8-eV spectrum shows that the thickness of the amorphous layer is substantially larger for the 8-eV film compared to the 12-eV film.

In order to probe the effect of energy on the quality of the IBE films deposited at constant temperature, films of ~20-nm thickness were deposited over the range $E=8$–80 eV for $T=160$ and 290 °C. The number of defects N_d in

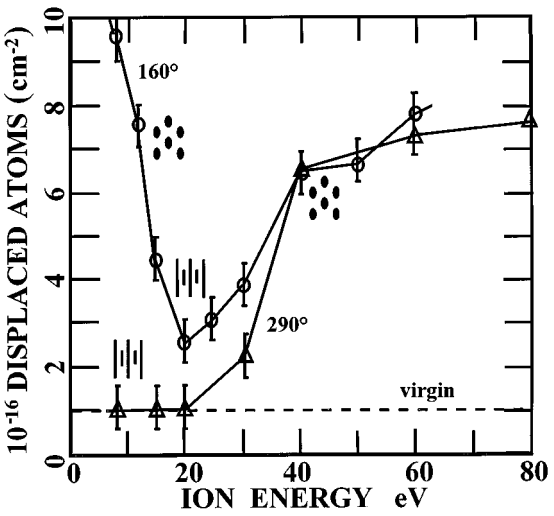

FIG. 12. Plot of the number of displaced atoms (N_d) in the silicon films vs $^{28}Si^+$ ion energy in films deposited at 160 and 290 °C. Qualitative sketches of RHEED patterns observed during growth are also shown. The number of displaced atoms observed in the virgin spectrum is 1×10^{16} cm^{-2}.

these films is plotted as a function of energy in Fig. 12. Qualitative sketches of the corresponding RHEED images observed during growth are also indicated in the figure. The plot obtained at 200 °C shows that N_d decreases sharply with increasing energy at low energy, reaches a minimum at $E\sim20$ eV, and then increases sharply with increasing energy at higher energy. This indicates that the optimum energy for epitaxial growth at 160 °C is 20 eV. Streaky (2×1) RHEED patterns were observed at 20 and 25 eV compared to 3D patterns at both lower and higher values of energy. The streaky patterns persisted for the entire film thickness, while the 3D patterns gave way to diffuse images at various doses (thicknesses), depending on energy. This indicates layer-by-layer growth at 20 and 25 eV. For $E<20$ eV or $E>25$ eV, the patterns are indicative of island growth and/or highly defective films followed by transition to an amorphous phase. For $E<20$ eV, the dose at which the crystalline-amorphous transition occurs decreases with decreasing energy, while for $E>20$ eV this dose increases with increasing energy. These results provide clear evidence for ion-beam-enhanced epitaxial growth of silicon, which is optimized at $E\sim20$ eV. The plot at $T=290$ °C shows that N_d is constant and very small in the range below 20 eV; our lowest data point is 8 eV. The defect density in these films increases rapidly with energy above 20 eV and at a lower rate above 40 eV. Here also, streaky patterns at $E\leqslant30$ eV and 3D spots at $E\geqslant30$ eV were observed; the 3D spots persisted to the end of deposition. The results of Fig. 12 are also in agreement with the TEM results of Fig. 5–8; i.e., the high crystalline quality films obtained at 160 °C/20 eV and 290 °C/15 eV correspond to the minima of Fig. 12.

D. SIMS results

A SIMS depth profile was carried out on a 325-nm-thick film deposited from $^{28}Si^+$ ions at 20 eV and on a 350 °C natural silicon substrate in order to monitor the isotropic purity of the film and the sharpness of the isotropic interface

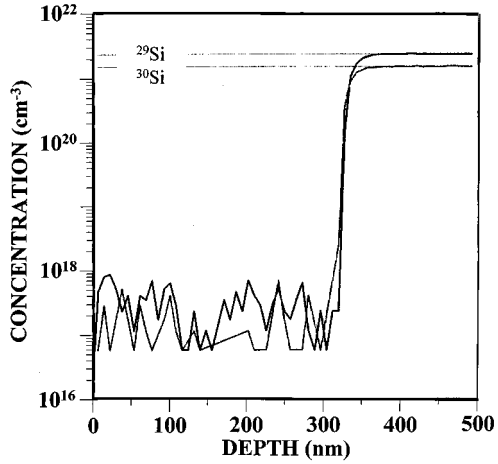

FIG. 13. SIMS depth profile of the minority silicon isotopes ^{29}Si and ^{30}Si using 2-keV Cs^+ ions for bombardment. The region above 325 nm corresponds to the native silicon substrate.

with the substrate. The depth profile was obtained by monitoring the ^{29}Si and ^{30}Si signals as a function of sputtering time using 10-keV Cs^+ ions. The data are plotted in Fig. 13 as the concentration of ^{29}Si and ^{30}Si as a function of depth below the film surface. The results show that the film is ~325 nm thick, and that the concentration of the ^{29}Si and ^{30}Si isotopes is lower than the SIMS detection limit; i.e., the signals for these minor isotopes are in the noise level. The concentrations of these minor isotopes rise sharply at the film-substrate interface, where they resume their normal levels of 4.67% and 3.10% for ^{29}Si and ^{30}Si, respectively, in the natural silicon substrate. The isotopic enhancement in the deposited film is $^{28}Si\,(^{29}Si+{}^{30}Si)>10^4$. The vertical rise in the concentrations of the minor impurities at the interface shows that the width of the interface is less than the vertical resolution of the SIMS depth profile. Therefore, the interface width cannot be determined by the SIMS depth profiling technique. These results show that the IBE technique is capable of depositing isotopically structured materials with well-defined interfaces.

IV. DISCUSSION

A. Summary of experimental results

The results reported in the previous section have established the following facts concerning silicon IBE.

(1) The growth mode, crystalline quality, and number of defects in the films are extremely sensitive to both substrate temperature (at low temperature) and ion energy (at low energy).

(2) Layer-by-layer growth has been observed down to ~160 °C with appropriate ion energies; below this temperature, island growth with transition to an amorphous phase occurs.

(3) There is an optimum ion-energy window for achieving layer-by-layer epitaxial growth and high crystalline quality films which are relatively defect free. This energy window is extremely narrow at low temperature, i.e., $\sim20\pm10$ eV at 160 °C, and broadens out particularly on the low-energy side

at higher temperatures, e.g., at 290 °C. The number of defects in the films increases significantly for energies >25 eV at both of these temperatures.

(4) For the conditions 290 °C and 20 eV, epitaxial films with crystalline quality equivalent to that of the bulk single-crystal substrate have been grown. The thickest films deposited were ~ 325 nm, and there was no indication of a limiting epitaxial layer thickness (h_{epi}).

(5) The IBE growth rate (0.7–1.4 Å/min) obtained at 290 °C and 20 eV is ~ 200 times higher than the solid-phase epitaxial growth rate[42] of silicon. This growth rate is limited by our present ion fluence limitations.

(6) The underlying silicon substrates contain no observable damage by TEM under the IBE conditions used.

(7) Isotopically structured epitaxial films with well-defined interfaces can be grown by IBE.

B. Ion-surface interactions that effect epitaxial growth

It is apparent from the above results that the dominant processes in the ion-surface interactions which control the kinetics and mechanisms and the defect formation and annihilation during silicon IBE are changing as ion energy is increased at low temperature. There are several different processes, some of which facilitate low-temperature epitaxy, and others which have deleterious effects that need to be considered. Molecular-dynamics simulations[27–34] of such low-energy ion-surface interactions have been extremely helpful in delineating these processes.

For atoms or ions with thermal energies colliding with a surface, there are three sources by which energy is introduced into the localized region of the collision site. First, the kinetic energy, albeit small (< 0.1 eV), of the impinging atoms is transferred to the lattice as phonon excitations. Second, slow Si^+ ions approaching a silicon surface are efficiently neutralized[43] prior to impact with the lattice atoms by resonant electronic charge exchange. The electronic energy introduced by this exchange is of the order of the ionization potential of silicon, i.e., 8.15 eV. This is sufficient to excite atoms in the collision region into excited electronic states, thereby weakening their bond energies and enhancing their mobilities. Third, the latent heat of condensation is released at the collision site as the incoming atoms bond to lattice atoms. The enthalpy of condensation of silicon is ~ 4 eV/atom, although the amount of this energy that is converted to kinetic or thermal energy depends on the number of bonds made in the condensation step.

As ion energy increases above the level of chemical bond energies, ~ 5–10 eV, sufficient momentum is transferred to the lattice atoms such that transient, localized atomic displacement and temperature spikes are created within which the probabilities of processes which are conducive to epitaxial growth are enhanced. These processes include rupture of chemical bonds, subsurface penetration, phonon and electron excitations, local atomic rearrangements, atomic displacements which create mobile vacancies and interstitials, and enhanced diffusion. We will consider these processes. The low-energy ions are capable of penetrating into subsurface sites[44] and the trapping probabilities of 8–80-eV Si^+ ions on Si{100} are near unity.[31] Si^+ ions at 10 eV have been shown[31] to stop in positions from an epitaxial bridge site above the surface dimers down to the fourth layer; the average stopping position was 0.5 Å below the surface, i.e., between the first and second layers. At 50 eV, the average stopping distance below the surface was 1.6 Å, i.e., between the second and third layers. This subsurface penetration produces collision sequences which result in local atomic rearrangements. Displacement threshold energies for Si^+ on Si{100} have been found[45] to range from ~ 10 to 22 eV depending on the orientation of the incident ion beam with respect to the crystallographic directions; 15 eV is taken as an average value. The collisions can result in opening of dimers, thus providing 1×1 growth sites for migrating atoms.[31] Stable Frenkel pair formation will be dependent on the vacancy-interstitial separation. It has been shown[27] that two types of Frenkel pairs are formed in such low-energy collision sequences. Close Frenkel pairs have a separation of only ~ 2.3 Å, a recombination barrier of ~ 1.0 eV, and consequently a lifetime of only ~ 0.2 μs. Extended Frenkel pairs have a separation of ~ 4.5 Å; although this constitutes an isolated vacancy-interstitial pair, they remain sufficiently close so that recombination through thermal motion can occur. The alterations in the lattice caused by the displacements, Frenkel pairs, and induced strain result in a surface with localized regions of high-energy content in which the defects are mobile. When the equilibrium concentration of these mobile defects is sufficient to induce ordered recrystallization, epitaxial growth at low temperature is facilitated.[46]

As ion energy continues to increase above the displacement threshold energy, the collision sequences become sufficiently energetic such that processes which are deleterious to epitaxial growth begin to dominate. Such processes include large vacancy-interstitial separations which result in permanent defect formation, lattice damage, sputtering, and atomic mixing. For example, molecular-dynamics simulations[31] have shown that raising the Si^+ ion energy from 10 to 50 eV for deposition on Si{100} results in a decrease in the ratio of the number of epitaxial events to the number of residual bulk defects from 63% to 21%. Sputtering events also begin to be observed at the high-energy side of this range. When the concentration of permanent defects induced by the ion beam exceeds the equilibrium concentration of the mobile defects, failure of epitaxial growth occurs and amorphization begins to take place.

C. Dynamic processes responsible for the observed energy/temperature features

The features observed in the plots of Figs. 11 and 12 are a manifestation of the dynamic processes discussed above. Ion-beam enhancement of epitaxy at low temperature occurs in an energy window which is determined by the specific dominating processes under those conditions. For deposition at energies less than ~ 8 eV, atomic displacements, local atomic rearrangements, and enhancement of mobilities are minimal. The adatoms, i.e., primary ions, and atoms neighboring the collision site may not be sufficiently mobile to migrate to the preferred sites, such as step edges, for layer-by-layer growth. This results in the nucleation of 3D islands on the terraces and accumulation of strain and permanent defects, followed by transition to amorphous phase at larger

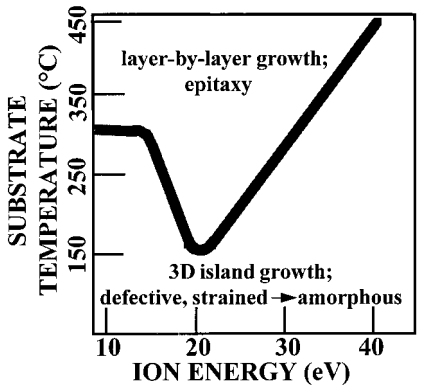

FIG. 14. Substrate temperature vs ion-energy phase diagram for silicon homoepitaxy.

thicknesses (Figs. 2–5, 9, and 10). The mobility of adatoms can be increased by increasing either the temperature or energy. The former may be the reason for the higher crystalline quality of the 290 °C films over the 160 °C films (Figs. 5 and 8). As energy increases in the range 10–35 eV, penetration and local displacements increase and the original Si^+ ion as well as Si atoms neighboring the collision site can acquire sufficient energy for mobility enhancement. When this enhancement is sufficient to overcome surface diffusion barriers,[47,48] the atoms are able to reach sites, such as step edges, which are conducive to layer-by-layer epitaxial growth. The energy transferred during the collisions may also lead to the fragmentation of clusters formed during growth.[12] As ion energy increases above ~35 eV, the infliction of permanent damage to the lattice increases more rapidly than the annealing processes are capable of healing, resulting in a sharp increase in the number of observed defects (Fig. 12). As a result, at temperatures below ~200 °C, the energy window for silicon IBE is in the range 10–35 eV. At temperatures near 290 °C, the mobility may be sufficiently high such that mobility enhancement by ion bombardment is not as critical as it is at 160 °C, resulting in the insensitivity of the number of displacements to ion energies below ~20 eV (Fig. 12). It is noted that the damage produced at energies greater than 40 eV at both temperatures is almost the same and relatively constant, even at 290 °C. This temperature may be too low for any significant annealing of the more extensive damage that is produced at the higher ion energies.

Based on the results obtained and the above discussion, it is possible to draw a substrate temperature versus Si^+ ion-energy phase diagram for silicon homoepitaxy as shown in Fig. 14. An approximate boundary line has been drawn between the regions where layer-by-layer epitaxial growth and island growth of defective, strained, and/or amorphous films have been observed. A distinct minimum is observed near 20 eV and 160 °C. This phase diagram may be applicable to silicon growth by other techniques which include energetic or accelerated particles. However, it is expected that several parameters, such as condition of the initial substrate surface, type of substrate (for heteroepitaxy), ion-dose rate, ion-energy spread, and contamination may affect the shape and position of the boundary in Fig. 14. The crystalline-amorphous transition in silicon homoepitaxy is known to be influenced by the presence of hydrogen and other contaminants.[7,36–38] It is expected that this problem is minimized in our case due to the UHV conditions[39] (H_2 partial pressure $<3\times10^{-9}$ mbar), low sticking coefficient of H_2, and absence of hot filaments in line of sight with the surface. However, a systematic study performed as a function of H_2 partial pressure may be needed to determine the role of hydrogen in silicon IBE. The technique of rapid thermal annealing (RTA) (Refs. 37 and 49) has not been applied to these IBE films. It is expected that RTA treatments, carried out at regular incremental doses during deposition, would significantly reduce the epitaxial temperatures obtained herein through annealing of the strained regions that induce transition to the amorphous phase.

V. CONCLUSIONS

Epitaxial silicon films with crystalline quality equivalent to the single-crystal substrate, sharp film-substrate interfaces, and isotopic purity have been grown by controlled $^{28}Si^+$ ion-beam epitaxy (IBE) at temperatures down to 160 °C. The crystalline quality exhibits a high sensitivity to both the ion-beam energy and substrate temperature. A sharp minimum observed in the number of defects in the films versus ion energy provides clear evidence of ion enhancement of epitaxial growth within an optimum energy window. This behavior is a result of changes in the dynamic processes which dominate the film growth mechanism as a function of ion energy and temperature. As ion energy increases above the level of bond energies, up to the atomic displacement threshold, and to more energetic levels, processes conducive to epitaxy such as subsurface penetration, local atomic rearrangements, Frenkel pair creation, and enhanced mobility are replaced by processes which are deleterious to epitaxy such as permanent defect formation, lattice damage, sputtering, and atomic mixing. As temperature increases, thermal vibrations, atomic mobility, and the ability to anneal the Frenkel pairs are enhanced, so that the sharp energy dependence observed at low temperature is broadened as temperature increases. The role of ion energy and substrate temperature in epitaxial growth, as elucidated herein by IBE, is directly relevant to other film growth processes which use energetic particles, e.g., ion-assisted MBE and plasma and sputter deposition techniques. This work also provides the basis for experiments with isotropically controlled silicon bulk crystals and $^{28}Si/^{30}Si$ superlattices. The latter can be doped *n* type in the ^{30}Si layers by neutron transmutation doping (NTD).

ACKNOWLEDGMENTS

The authors are grateful to E. E. Haller and L. Wang for SIMS depth profile analysis conducted at Charles Evans & Assoc. This material was based on work supported by the National Science Foundation under Grant No. DMR-9224377 and the R. A. Welch Foundation under Grant No. E656.

*Author to whom correspondence should be addressed.

[1] P. C. Zal and L. J. Beckers, Appl. Phys. Lett. **41**, 167 (1982).

[2] R. A. Zuhr, G. D. Alton, B. R. Appleton, N. Herbots, T. S. Noggle, and S. J. Pennycook, in *Materials Modification and Growth Using Ion Beams*, edited by O. Gibson, A. E. White, and P. P. Pronko, MRS Symposia Proceedings No. 43 (Materials Research Society, Pittsburgh, 1987); B. R. Appleton, R. A. Zuhr, T. S. Noggle, N. Herbots, and S. J. Pennycook, in *Beam Solid Interactions and Transient Processes*, edited by M. O. Thompson, S. T. Picraux, and J. S. Williams, MRS Symposia Proceedings No. 74 (Materials Research Society, Pittsburgh, 1987); p. 45; R. A. Zuhr, S. J. Pennycook, T. E. Haynes, and O. W. Holland, in *Processing and Characterization of Materials Using Ion Beams*, edited by L. E. Rehn, J. Greene, and F. A. Smidt, MRS Symposia Proceedings No. 128 (Materials Research Society, Pittsburgh, 1989), p. 128; T. E. Haynes, R. Z. Zuhr, and S. J. Pennycook, in *Advances in Materials, Processing and Devices in III-V Compound Semiconductors*, edited by D. K. Sadana, L. Eastman, and R. Dupuis, MRS Symposia Proceedings No. 144 (Materials Research Society, Pittsburgh, 1989), p. 311.

[3] R. A. Zuhr, B. R. Appleton, N. Herbots, B. C. Larson, T. S. Noggle, and S. J. Pennycook, J. Vac. Sci. Technol A **5**, 2135 (1987); R. A. Zuhr, S. J. Pennycook, T. S. Noggle, N. Herbots, T. E. Haynes, and B. R. Appleton, Nucl. Instrum. Methods Phys. Res. Sect. B **37/38**, 16 (1989); S. P. Withrow, K. L. More, R. A. Zuhr, and T. E. Haynes, Vacuum **39**, 1065 (1989); T. E. Haynes, R. A. Zuhr, S. J. Pennycook, and B. R. Appleton, Appl. Phys. Lett. **54**, 1439 (1989).

[4] N. Herbots, B. R. Appleton, T. S. Noggle, R. A. Zuhr, and S. J. Pennycook, Nucl. Instrum. Methods Phys. Res. B **13**, 250 (1986).

[5] K. J. Orrman-Rossiter, A. H. Al-Bayati, D. G. Armour, S. E. Donnely, and J. A. van den Berg, Nucl. Instrum. Methods Phys. Res. Sect. B **59/60**, 197 (1991); K. G. Orrman-Rossiter, D. R. G. Mitchell, S. E. Donnelly, C. J. Rossouw, S. R. Glanvill, P. R. Miller, A. H. Al-Bayati, J. A. van den Berg, and D. G. Armour, Philos. Mag. Lett. **61**, 311 (1990).

[6] A. H. Al-Bayati, K. J. Boyd, D. Marton, S. S. Todorov, J. W. Rabalias, Z. H. Zhang, and W. K. Chu, J. Appl. Phys. **76**, 4383 (1994); A. H. Al-Bayati, S. S. Todorov, K. J. Boyd, D. Marton, and J. W. Rabalais, J. Vac. Sci. Technol. B **13**, 1639 (1995).

[7] The temperature scales used in the data of Ref. 6 have been found to be consistently too high. The recalibrated values are as follows: the temperatures in Ref. 6 listed as 350°, 200°, and 50° should be changed to 290°, 160°, and 40°, respectively.

[8] K. Miyake, in *Beam-Solid Interactions: Physical Phenomena*, edited by J. A. Knapp, P. Bøgesen, and R. A. Zuhr, MRS Symposia Proceedings No. 157 (Materials Research Society, Pittsburgh, 1987), p. 92; K. Miyake and T. Tokuyama, Thin Solid Films **92**, 123 (1982).

[9] M. Matsuoka and S. Tohno, J. Vac. Sci. Technol. A **13**, 305 (1995).

[10] M. V. R. Murty, H. A. Atwater, A. J. Kellock, and J. E. E. Baglin, Appl. Phys. Lett. **62**, 2566 (1993).

[11] T. Ohmi, T. Ichikawa, H. Iwabuchi, and T. Shibata, J. Appl. Phys. **66**, 4756 (1989).

[12] C.-H. Choi, L. Hultman, and S. A. Barnett, J. Vac. Sci. Technol. A **8**, 1587 (1990).

[13] M. V. R. Murty and H. A. Atwater, Phys. Rev. B **49**, 8483 (1994).

[14] S. Aisenberg and R. Chabot, J. Appl. Phys. **42**, 2953 (1971).

[15] R. B. Fair, J. Appl. Phys. **42**, 3176 (1971).

[16] J. Amano, Thin Solid Films **92**, 115 (1982); J. Amano and R. P. W. Lawson, J. Vac. Sci. Technol. **14**, 831 (1977); J. Amano, P. Bryce, and R. P. Lawson, *ibid.* **13**, 591 (1976).

[17] K. Yagi, S. Tamura, and T. Tokyama, Jpn. J. Appl. Phys. **16**, 245 (1977).

[18] T. Miyazawa, S. Misawa, S. Yoshida, and S. Gonda, J. Appl. Phys. **55**, 188 (1984); T. Miyazawa, S. Yoshida, S. Misawa, S. Gonda, and J. Ohdomari, Appl. Phys. Lett. **45**, 380 (1984).

[19] S. Tamura, M. Hyouzho, K. Yokota, and S. Katayama, Nucl. Instrum. Methods Phys. Res. Sect. B **37/38**, 862 (1989).

[20] S. R. Kasi, H. Kang, and J. W. Rabalais, Phys. Rev. Lett. **59**, 75 (1987); J. Chem. Phys. **88**, 5914 (1988); J. Vac. Sci. Technol. A **6**, 1788 (1988); S. R. Kasi, M. A. Kilburn, H. Kang, J. W. Rabalais, L. Tavernini, and P. Hochmann, J. Chem. Phys. **88**, 5902 (1988).

[21] Y. Lifshitz, G. D. Lempert, S. Rotter, I. Avigal, C. Uzan-Saguy, R. Kalish, J. Kulik, D. Marton, and J. W. Rabalais, Diamond Relat. Mater. **3**, 542 (1994).

[22] Y. Lifshitz, G. D. Lempert, and E. Grosman, Phys. Rev. Lett. **72**, 2759 (1994).

[23] C. Weissmantel, J. Vac. Sci. Technol. **18**, 179 (1981).

[24] T. Ohnishi, Y. Yoshida, Y. Hirofuji, and H. Iwasaki, Nucl. Instrum. Methods Phys. Res. Sect. B **37/38**, 850 (1989); Y. Yoshida, T. Ohnishi, Y. Hirofuji, H. Iwasaki, and T. Ikeda, *ibid.* **37/38**, 866 (1989).

[25] J. Y. Tsao, E. Chason, K. M. Horn, D. K. Brice, and S. T. Picraux, Nucl. Instrum. Methods Phys. Res. Sect. B **39**, 72 (1989).

[26] S. S. Todorov, D. Marton, K. J. Boyd, A. H. Al-Bayati, and J. W. Rabalais, J. Vac. Sci. Technol. A **12**, 3192 (1994).

[27] L. A. Miller, D. K. Brice, A. K. Prinja, and S. T. Picraux, Radiat. Eff. Def. Solids **129**, 127 (1994); Phys. Rev. B **49**, 16 953 (1994).

[28] Z. Zhang and H. Meitiu, Surf. Sci. **245**, 353 (1991).

[29] R. Smith, R. Tsu, T. R. Bramblett, and J. E. Greene, Phys. Rev. B **40**, 93 (1989).

[30] B. W. Dodson, Solid State Mater. Sci. **16**, 115 (1990).

[31] M. Kitabatake, P. Fons, and J. E. Greene, J. Vac. Sci. Technol. A **8**, 3726 (1990).

[32] H.-P. Kaukonen, and R. M. Nieminen, Phys. Rev. Lett. **68**, 620 (1992).

[33] J. A. Sprague and C. M. Gilmore, in *Materials Modification by Energetic Atoms and Ions*, edited by K. S. Grabowski *et al.*, MRS Symposia Proceedings No. 268 (Materials Research Society, Pittsburgh, 1992).

[34] T. Ohashi, K. Miyake, and K. Ohashi, Nucl. Instrum. Methods Phys. Res. Sect. B **91**, 593 (1994).

[35] D. J. Eaglesham, H.-J. Gossmann, and M. Cerullo, Phys. Rev. Lett. **65**, 1990 (1990).

[36] D. P. Adams, S. M. Yalisove, and D. J. Eaglesham, Appl. Phys. Lett. **63**, 3571 (1993); D. J. Eaglesham, J. Appl. Phys. **77**, 3597 (1995).

[37] P. Asoka-Kumar, S. Szpala, B. Nielsen, Cs. Szeles, and K. G. Lynn, W. A. Lanford, C. A. Shepard, and H.-J. Gossmann, Phys. Rev. B **51**, 4630 (1995).

[38] S. H. Wolff, S. Wagner, J. C. Bean, R. Hull, and J. M. Gibson, Appl. Phys. Lett. **55**, 2017 (1989).

[39] A. H. Al-Bayati, D. Marton, S. S. Todorov, K. J. Boyd, J. W. Rabalais, D. G. Armour, J. S. Gordon, and G. Duller, Rev. Sci. Instrum. **65**, 2680 (1994).

[40] R. J. Hamers, R. M. Tromp, and J. E. Demouth, Phys. Rev. B **34**, 5343 (1986).

[41] W. K. Liu, S. M. Mokler, N. Ohtani, C. Roberts, and B. A. Joyce, Surf. Sci. **264**, 301 (1992); C.-H. Choi, R. Ai, and S. A. Barnett, Phys. Rev. Lett. **67**, 2826 (1991); S. V. Hattangady, J. B. Posthill, G. G. Fountain, R. A. Rudder, M. J. Mantini, and R. J. Markunas, Appl. Phys. Lett. **59**, 339 (1991).

[42] J. A. Roth, G. L. Olson, D. C. Jacobson, and J. M. Poate, Appl. Phys. Lett. **57**, 1340 (1990); L. Csepregi, J. W. Mayer, and T. W. Sigmon, Phys. Lett. **54A**, 157 (1975).

[43] J. W. Rabalais, J. N. Chen, R. Kumar, and M. Narayana, J. Chem. Phys. **83**, 6489 (1985).

[44] Y. Lifshitz, S. R. Kasi, and J. W. Rabalais, Phys. Rev. Lett. **62**, 1290 (1989); Phys. Rev. B **41**, 10 468 (1990).

[45] D. Marton in *Low Energy Ion-Surface Interactions*, edited by J. W. Rabalais (Wiley, Chichester, 1994), p. 525.

[46] K. A. Jackson, J. Mater. Res. **3**, 1218 (1988).

[47] Y. T. Lu, Z. Zhang, and H. Metiu, Surf. Sci. **257**, 199 (1991).

[48] G. Brocks, P. J. Kelly, and R. Car, Phys. Rev. Lett. **66**, 1729 (1991).

[49] E. K. F. Dang and R. J. Gooding, Phys. Rev. Lett. **74**, 3848 (1995).